Novel low-temperature and high-flux hydrogen plasma source for extreme-ultraviolet lithography applications © •

Special Collection: CHIPS: Future of Semiconductor Processing and Devices

A. S. Stodolna D : T. W. Mechielsen : P. van der Walle : C. Meekes : H. Lensen



J. Vac. Sci. Technol. B 42, 052601 (2024) https://doi.org/10.1116/6.0003701









Novel low-temperature and high-flux hydrogen plasma source for extreme-ultraviolet lithography applications 💿 🙃

Cite as: J. Vac. Sci. Technol. B 42, 052601 (2024); doi: 10.1116/6.0003701 Submitted: 18 April 2024 · Accepted: 10 July 2024 · Published Online: 6 August 2024







A. S. Stodolna, a) 📵 T. W. Mechielsen, 📵 P. van der Walle, 📵 C. Meekes, 📵 and H. Lensen

AFFILIATIONS

TNO, P.O. Box 155, Delft 2600AD, The Netherlands

Note: This paper is a part of the Special Topic Collection: CHIPS: Future of Semiconductor Processing and Devices.

a) Author to whom correspondence should be addressed: aneta.stodolna@tno.nl

ABSTRACT

Inside extreme-ultraviolet (EUV) lithography machines, a hydrogen plasma is generated by ionization of the background gas by EUV photons. This plasma is essential for preventing carbon build-up on the optics, but it might affect functional performance and the lifetime of other elements inside the machine. The interaction of scanner materials and components with hydrogen plasma is investigated in controlled experiments using laboratory (off-line) setups, where the properties of EUV-generated plasmas are mimicked. Here, we present a novel experimental setup at TNO, where a low-temperature hydrogen plasma is generated by means of electron-impact ionization using a generated by means of electron-impact ionization using a high-current, high-pressure electron beam (e-beam) gun. We show that the produced ion flux, peak ion energies, and radical-to-ion ratio are similar to that of the EUV-generated plasma. Since the e-gun has the option of operating the e-gun in the pulsed mode, it is possible to reproduce the time-dependent behavior of the scanner plasma as well. Moreover, as shown by Luo et al. [RSC Adv. 10, 8385 (2020)], electrons that impinge on surfaces mimic EUV photons in the generation of secondary electrons, which often drive radiation-induced processes $\hat{\mathfrak{A}}$ (e.g., surface oxidation, reduction, and growth of carbon). We conclude that e-beam generated hydrogen plasma is a very promising technology for cost-effective lifetime testing of materials and optics, as compared to setups with EUV sources.

© 2024 Author(s). All article content, except where otherwise noted, is licensed under a Creative Commons Attribution (CC BY) license (https://creativecommons.org/licenses/by/4.0/). https://doi.org/10.1116/6.0003701

I. INTRODUCTION

Extreme-ultraviolet (EUV) lithography is the leading technology used in the semiconductor industry for printing the finest structures with nanometer resolution for the most advanced microchips. It uses light at the extremely short wavelength of 13.5 nm to image structures from a patterned photomask onto a photoresistcoated silicon wafer. EUV radiation is highly absorbed by nearly all matter. As a consequence, the beam path from the EUV source to the wafer needs to be in near-vacuum. The scanner is filled with a few pascals of H₂ gas to ensure self-cleaning conditions for EUV optics,^{2,3} preventing surface contamination and consequently EUV reflectivity loss. Due to the presence of H2 gas, a low-temperature, low-density hydrogen plasma is generated along the EUV beam path.2 It is essential to investigate the properties of the EUV-generated hydrogen plasma in order to emulate it in

laboratory setups, where its interaction with EUV optics, components, and relevant scanner materials can be studied in controlled experiments. The key parameters to reproduce in these off-line setups are ion flux, radical flux, radical-to-ion ratio, ion energy, and EUV photons. Various types of plasma sources, like microwave plasma sources or electron cyclotron resonance (ECR) sources, might be used to mimic EUV-generated hydrogen plasma. However, such sources lack EUV photons and produce ions with higher kinetic energies. Additionally, active elements in the plasma chamber (e.g., antennas) may cause contamination. Another possibility is to use more complex setups equipped with an actual EUV source. Laser-produced plasma sources, laser-assisted discharge plasma sources [like the EUV Beam Line 2 (EBL2) facility at TNO (Ref. 4)], synchrotron radiation, and free electron lasers can be considered here. This approach will likely lead to plasma conditions more representative of plasma conditions in lithography

equipment, as compared to plasma setups without EUV.² Nevertheless, EUV setups are scarce, complex and require more resources to operate. This makes them not ideal for cost-efficient research and development on plasma-material interaction.

In the past, electron beams have been used to generate plasmas with unique properties: high plasma densities (10¹⁶- $10^{18} \,\mathrm{m}^{-3}$), low electron temperatures ($\leq 1 \,\mathrm{eV}$), and low ion kinetic energies (≤5 eV). Etching, 6,7 nitriding, 8 thin film deposition, 9 and material processing 10,11 have been considered as applications. Moreover, in e-beam generated plasmas, ion fluxes, ionic species ratios, or radical-to-ion ratios can be adjusted in a controlled way by varying the distance with respect to the electron beam, gas composition, 11 or duty cycle. 12 The high plasma density, low ion kinetic energy, and tunability of plasma species are of particular interest for mimicking the key properties of EUV-generated hydrogen plasmas. Additionally, primary electrons in the electron beam generate secondary electrons on surfaces with a similar energy spectrum as the secondary photoelectrons produced by EUV photons. 13 Electron beams have been used to emulate EUV-induced oxidation¹⁴ and EUV-induced carbon deposition.¹⁵ Finally, as described by van de Kerkhof et al., pulsed-EUV sources produce a "dynamic" plasma that varies in time. Consequently, the ion flux and the ion energy distribution function (IEDF) will vary in time in pulsed-EUV setups. Continuous-wave plasma sources (e.g., ECR) reproduce the time-averaged fluxes and IEDF at best, but do not reproduce the dynamical effects. This potential issue can be solved using electron-beam-generated plasmas, which can be operated in pulsed mode with adjustable pulse duration and repetition rate.

In this paper, we present a novel plasma setup that uses electron-impact ionization to mimick key properties of EUV-generated hydrogen plasma. Plasma generation is feasible at H₂ gas pressures between 1 and 10 Pa using a high-current, highpressure electron beam gun. We report a maximum ion flux of $\phi_{\rm ion} = 6 \times 10^{18} \ {
m m}^{-2} \, {
m s}^{-1}$ with a peak ion energy of 2 eV (for a continuous-wave operation) and a maximum recombining H radical flux of $\phi_{\text{rec},H} = 4 \times 10^{20} \text{ m}^{-2} \text{ s}^{-1}$. The measured radical-to-ion ratio is at least one order of magnitude higher compared to other off-line plasma setups and, therefore, better resembles the scanner conditions. Finally, by using the e-gun in the pulsed mode, we generated hydrogen plasma with a similar temporal behavior compared to the pulsed-EUV-generated plasma.

II. EXPERIMENTAL SETUP

Figure 1 shows a schematic cross-sectional view of the novel plasma setup at TNO called EBR (electron beam research). It consists of two differentially pumped vacuum chambers connected via a 10 mm orifice. A high-current, high-pressure electron beam gun (TES-63-ES, Polygon Physics) is mounted on the smaller vessel using a CF63 flange. This electron gun uses a miniature ECR plasma source, typically filled with gas in the 0.5-5 Pa pressure range, to produce electrons. In current experiments, H2 gas is used. Other gasses may also be used, e.g., N2 or Ar. The advantage of using a plasma as a source of electrons is that the e-gun can be operated at relatively high chamber pressures up to a few pascal, unlike filament-based electron-guns which require much lower

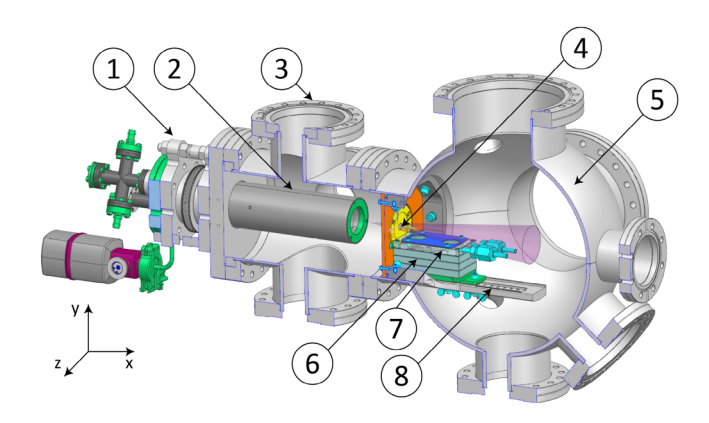


FIG. 1. Schematic cross-sectional view of the EBR setup containing a port aligner (1) used for mounting an e-gun (2) onto a smaller vacuum vessel (3), which is connected via a 10 mm orifice (4) with a main, exposure chamber (5). A sample stage (6) consist of three 1 cm spacers and a top, water-cooled plate (7), which has openings for two 1-in. samples. The stage is positioned on a rail (8), which allows for stage movement along the x axis.

pressure during operation. The high-pressure e-gun simplifies the experimental setup considerably w.r.t. filament-based e-gun setups. It consists of just two differentially pumped stages. Much more complex solutions were needed to achieve the four orders of magnitude pressure suppression required for a filament-based e-gun (see our previous publication¹⁵). Ignition inside the ECR plasma cavity starts by applying 5 W of microwaves to the antenna. Subsequently, the electrons are extracted from the cavity using a bias voltage in the 0-3000 V range, which also accelerates them. A second bias voltage in the 0-3000 V range is applied to an Einzel lens that focusses the emitted electron beam through the 10 mm orifice. The $\ddot{\xi}$ alignment of the e-beam through the orifice was done mechanically using a port-aligner flange. A Faraday cup was installed in the second chamber during the alignment procedure, directly behind the orifice, to measure the e-beam current. A transmission larger than 92% was achieved after mechanical alignment and optimization of the Einzel lens. The electron beam current is controlled by a combination of gas pressure in the ECR plasma cavity and power applied to the antenna. In the current configuration, it was possible to obtain electron beam currents in the 0.1-30 mA range, close to the specified maximum current of 50 mA.

The second, larger vacuum chamber contains a water-cooled sample stage (elements 6 and 7 in Fig. 1), which faces the 10 mm orifice. The stage consists of a top block supported by three spacers, each with a thickness of 1 cm. The spacers can be removed to change the position of the stage in the y-direction with respect to the e-beam. The movement along the x-direction, i.e., away from the orifice, is achieved by using a rail underneath the sample stage assembly. The top block has two openings for mounting 1-in. samples in combination with a cover plate and threaded holes for clamping sensors for plasma characterization. The exposure chamber is pumped by a 180 l/s turbo molecular pump (Pfeiffer, TMU 2000M) and routinely reaches a base pressure of 2×10^{-6} Pa without baking. Hydrogen gas is injected into the chamber using a

mass-flow controller (Alicat MC500), typically in the 1-10 Pa range. Plasma generation starts immediately once the electron beam is injected into the exposure chamber filled with H2 gas and a purple glow can be observed through a viewport.

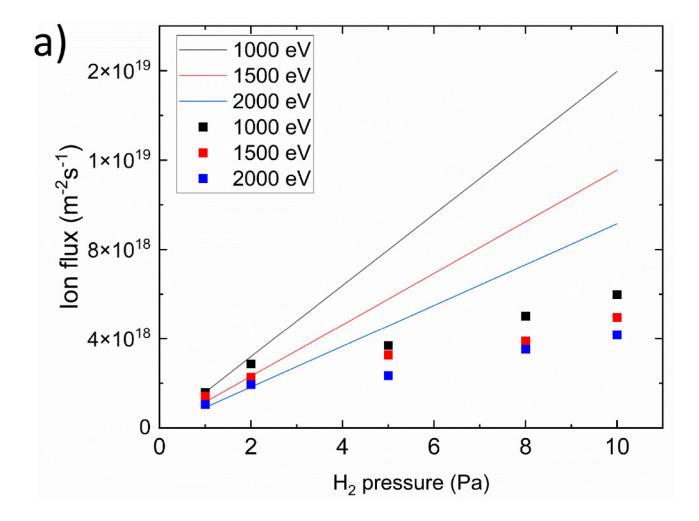
The cleanliness of a plasma setup is a critical parameter in material-testing experiments, where the interaction between samples and hydrogen plasma is investigated. Ideally, the experimental chamber is inert and free of any molecular contaminants to ensure the sample-under-test interacts solely with hydrogen plasma. In reality, hydrogen species present in the plasma may react with materials in the setup to produce molecular contaminants, a process denoted as "hydrogen-induced outgassing" or HIO. Specifically, reactions may produce volatile hydrides that can redeposit on the sample-under test. 16 In particular, elements like electrodes or antennas are potential sources of contamination, since they are often made of high-HIO-risk materials. Plasma-induced sputtering of electrodes¹⁵ may also give rise to contamination. A main advantage of the EBR setup is that the exposure chamber does not contain any plasma-generation hardware because the electron gun is mounted in a separate vacuum chamber coupled only by a small 10 mm orifice (see Fig. 1 for more details). The cleanliness of the EBR setup was measured using a Ru-coated sapphire test-sample. Ru was selected because of its excellent atomic and molecular adsorption properties.¹ The sample was positioned in the EBR setup and exposed to hydrogen plasma for 8 h, resulting in a total ion dose of $1.7\times10^{23}\,\text{m}^{-2}$. After the exposure, the sample surface was measured with x-ray photoemission spectroscopy. The data showed minor trace contamination of elements Zn, Si, S, P, and Sn, with a total concentration of 3.4 at .% which is less than one atomic monolayer. In comparison to other off-line plasma setups at TNO, the cleanliness of the EBR setup is better than that of setups equipped with microwave or RF sources and similar to ECR setups. This cleanliness was considered sufficiently low for planned material tests. We expect that cleanliness can be improved further, e.g., using ultraclean metal shielding around the sample stage.

III. PLASMA CHARACTERIZATION

A. Ion fluxes (continuous vs pulsed operation)

The total ion flux was measured in an e-beam generated hydrogen plasma using a commercial retarding field energy analyzer (RFEA, Semion, Impedance). In the first series of measurements, the e-gun was operated in the continuous wave (CW) mode. The time-averaged ion flux was measured as a function of H2 gas pressure (1-10 Pa), electron beam current (10-27 mA), electron energy (500-2000 eV), and position of the RFEA with respect to the e-beam.

Figure 2(a) shows the ion fluxes (symbol colors) as measured by the RFEA positioned approximately 5 cm behind the 10 mm orifice (x-direction) and 1 cm below the e-beam (y-direction). These measurements were performed at a constant e-beam current of 27 mA with a variable electron energy in the 1000-2000 eV range. The measured ion fluxes increased with H₂ pressure. Measurements are compared to a simple model based on linear



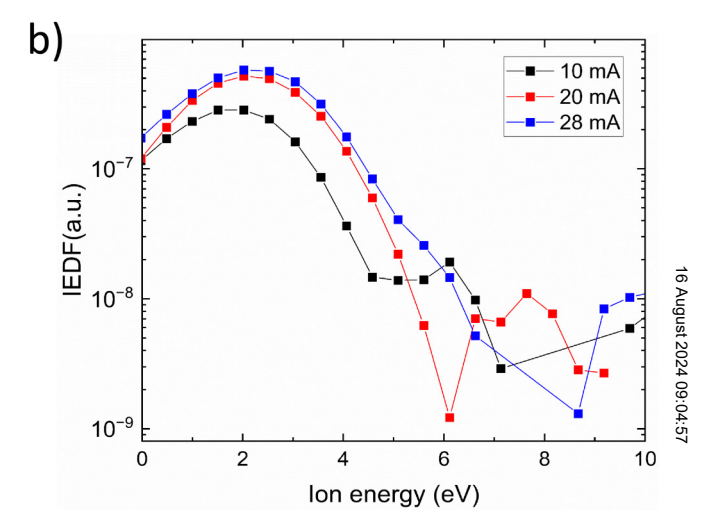


FIG. 2. (a) Measured ion fluxes for three different electron energies (symbol colors) as a function of H2 pressure inside the experimental chamber. Solid lines show the expected ion fluxes at the position of RFEA calculated with Eq. (1). (b) IEDF measured at 10 Pa of H₂ pressure and 1000 eV electron beam for different currents.

pressure scaling, see Ref. 18 for details,

$$\phi_{\text{ion,RFEA}} = \frac{I \cdot p_{\text{H}_2} \cdot \sigma_{\text{H}_2}}{e \cdot k_B \cdot T \cdot 2\pi y},$$
 (1)

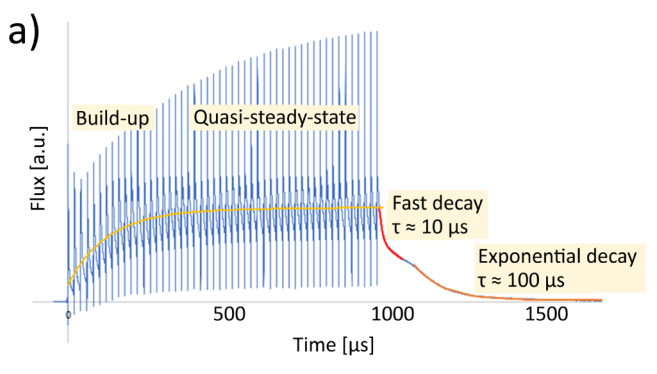
where I is the e-beam current, p_{H_2} is the hydrogen gas pressure, $\sigma_{\rm H_2}$ is the ionization cross-sectional area, e is the elementary charge, k_B is the Boltzmann constant, T is the absolute temperature, and y is the distance between the beam and the RFEA. The electron-impact ionization cross section for H2 used here is calculated based on the binary-encounter Bethe model. 19 The difference between calculated and measured ion fluxes is most likely due to

plasma recombination processes, which are not included in Eq. (1). This process was previously observed in ion flux measurements for an EUV-generated plasma, as shown in Ref. 2 (e.g., Fig. 14).

The highest ion flux of $\phi_{\rm ion} = 6 \times 10^{18}~{\rm m}^{-2}~{\rm s}^{-1}$ was measured using a 1000 eV electron beam at 10 Pa of H2 gas. At this pressure, the ion flux was also measured for electron energies of 1500 and 2000 eV. Increasing the electron energy resulted in a reduction of the ion flux as compared to the 1000 eV measurements. This observation is explained by a decreasing electron-impact ionization cross section with increasing electron energy. For electron energies below 1000 eV, we also observed a decrease in ion flux, even though the ionization cross section increases at these energies with a maximum around 70 eV. However, for lower electron energies other processes (e.g., hydrogen excitation and dissociation) have higher rates compared to the ionization.²⁰ Hence, the most optimum electron energy for plasma generation is around 1000 eV. Finally, we observed a linear increase of the ion flux with the e-beam current and a decrease along the x and y axes.

IEDF were acquired simultaneously with ion fluxes using the RFEA. Figure 2(b) shows IEDF's measured at 10 Pa of H₂ gas in the exposure chamber and using a 1000 eV electron beam. By varying the beam current from 10 to 28 mA, a small shift of the peak ion energy from approximately 2.0-2.5 eV was observed. A decrease in the peak ion energy from 2.5-2.0 eV was noticed when changing the hydrogen pressure from 5 to 1 Pa while keeping the beam current constant. Changes in electron beam energy and position along the x and y axes did not affect the IEDF. The observed ion energies of a few electron volts are characteristic for electron-beam-generated plasmas.⁵ A correlation is expected between the IEDF and the electron temperature.²¹ When a plasma is ignited and sustained by high-energy electrons, the plasma electrons quickly cool down, unlike in discharge plasmas, where external fields accelerate and thus heat up the electrons. Consequently, the electron temperature in e-beam generated plasmas is lower compared to discharge source plasmas. Additionally, in molecular gases, inelastic collisions between electrons and gas molecules provide an additional cooling mechanism resulting in an electron temperature below 1 eV.²² This mechanism also explains our observation that the peak ion energy decreases with increasing gas

In the second series of RFEA measurements, the e-gun was operated in pulsed mode to simulate the dynamic behavior of the pulsed-EUV-generated plasma. In the past, researchers from Advanced Semiconductor Materials Lithography (ASML) conducted time-resolved RFEA measurements on an EUV-setup equipped with a laser-produced plasma (LPP) source. This EUV source was similar to those used in EUV lithography machines.² The LPP source typically operates at 50 kHz, generating EUV pulses shorter than 100 ns. Each EUV pulse ignites a plasma that lasts tens of microseconds. At 50 kHz (20 µs between pulses), the plasma does not fully decay between consecutive pulses. This results in a plasma build-up that is observed for the first 10-20 pulses, followed by a quasi-steady state at longer time scales [see Fig. 3(a)]. Two types of plasma decay are observed after switching off the EUV source. We operated the electron gun in pulsed mode to simulate the dynamic behavior of the pulsed-EUV-generated plasma. Approximately 500 ns long pulses



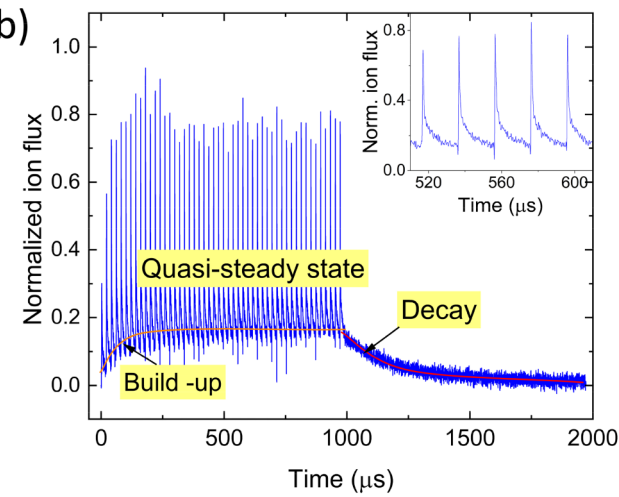


FIG. 3. Time-resolved ion flux measurements for (a) the pulsed-EUV-generated plasma in 5 Pa of H2 gas measured by ASML researchers. (a) is reproduced with permission from van de Kerkhof et al., J. Micro-Nanolith. MEMS MOEMS 20, 033801 (2021). Copyright 2021 Author(s), licensed under a Creative Commons License)2 and (b) the pulsed e-beam-generated plasma in 10 Pa of H₂ gas at the EBR setup. The inset shows consecutive pulses for the quasi-steady state.

were generated at a repetition rate of 50 kHz using an arbitrary waveform generator connected to the e-gun. Figure 3(b) shows time-resolved RFEA measurements for the resulting e-beam generated plasma in 10 Pa of hydrogen gas for a 1 ms pulse train (50 pulses). Results are qualitatively similar to the EUV-generated plasma case. We observe a build-up for the first few pulses followed by a quasi-steady state. In contrast to the EUV-generated plasma, a single decay process is visible in our pulsed e-beam plasma when the pulse train is finished. At this moment, the root cause for this observation is unknown. Time constants for the build-up and decay processes, which are driven by diffusion, are shorter for pulsed e-beam plasmas, as compared to pulsed-EUV plasmas. The cause is not clear yet, but we speculate that this is due to experimental differences, e.g., gas pressure (5 vs 10 Pa) and position of

the RFEA with respect to the electron beam. The inset in Fig. 3

shows consecutive pulses in the quasi-steady state, where small

pulse-to-pulse variations in the ion flux are observed. This effect is

caused by differing electron currents per electron pulse, which was confirmed by time-resolved measurements of the e-beam currents using the Faraday cup.

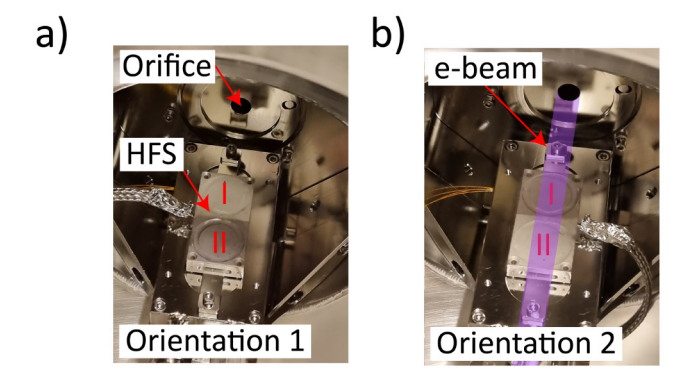
The time-resolved RFEA measurements at the EBR setup provided information on ion energy distribution functions as well. It was observed that the peak ion energy changes over time, showing relatively high values of approximately 10 eV at the beginning of the electron pulse. With time, the peak ion energy drops to roughly 2 eV, where it stays constant until the plasma is extinguished. A similar time-dependent behavior of the peak ion energy was observed in EUV-generated plasmas, where it also dropped to a metastable plateau of 2 eV, which was explained by superelastic collisions with vibrationally excited hydrogen molecules.

Follow up experiments are planned to further investigate effects of different electron pulse durations and repetition rates on the dynamic behavior of e-beam generated plasmas in hydrogen. The results confirm that e-gun plasma and EUV plasmas are highly similar. This strongly indicates the potential of e-beam plasmas for material and optics lifetime testing for EUV lithography applications.

B. Hydrogen (radical) flux

The recombining hydrogen (radical) fluxes were measured using a dual probe thermopile heat flux or radical sensor, in this paper referred to as HFS. The HFS was developed at TNO and its design, construction and application for measuring atomic hydrogen fluxes in a low-temperature plasma was described by Velthuis et al.²² In short, it provides quantitative information on the radicalrecombination flux $(\phi_{{
m rec},H})$ by measuring the heat released during recombination of hydrogen atoms on its surface. This approach requires discrimination between the radical-recombination heat flux and the so-called "background" heat loads (e.g., due to ions and electrons from the plasma and due to thermal radiation from the environment). A single heat-flux transducer cannot make this discrimination. Therefore, the HFS consists of two very similar sensors side-by-side, each coated with a material with a different recombination coefficient γ : HFS₁ is coated with $1 \mu m$ of Pt $(\gamma_{\rm Pt} \sim 0.3)^{23}$ and HFS₂ with 100 nm of Al₂O₃ $(\gamma_{\rm Al_2O_3} \sim 0.002)$. H-recombination occurs primarily on the Pt coating whereas on the Al₂O₃ side it can be neglected. By taking the differential signal $Q_{\Delta HFS} = Q_{HFS_1} - Q_{HFS_2}$, common-mode background heat loads are largely rejected and the impinging radical flux is proportional to the differential signal: $\phi_H \sim \frac{Q_{\rm AHFS}}{\gamma_{\rm Pl} - \gamma_{\rm Al_{\rm P}O_3}}$. The hydrogen recombination coefficient γ is a complex parameter that depends on the surface material and its state, like the presence of an oxide layer, 25 cleanliness,²⁶ or previous exposure to a plasma.²⁷ Therefore, reported literature values of γ for the same material can differ by orders of magnitude, which results in large uncertainties in the impinging radical flux. Since there is no information on the Pt recombination coefficient under a similar plasma heat load, here we report values of the recombining H flux ($\phi_{{
m rec},H}\sim Q_{\Delta {
m HFS}}$) only, not the total radical flux.

During measurements, the HFS was positioned parallel to and approximately 1 cm below the electron beam, similar to the RFEA measurements. To avoid any effects of inhomogeneous H fluxes and background heat loads along the HFS, the measurements were



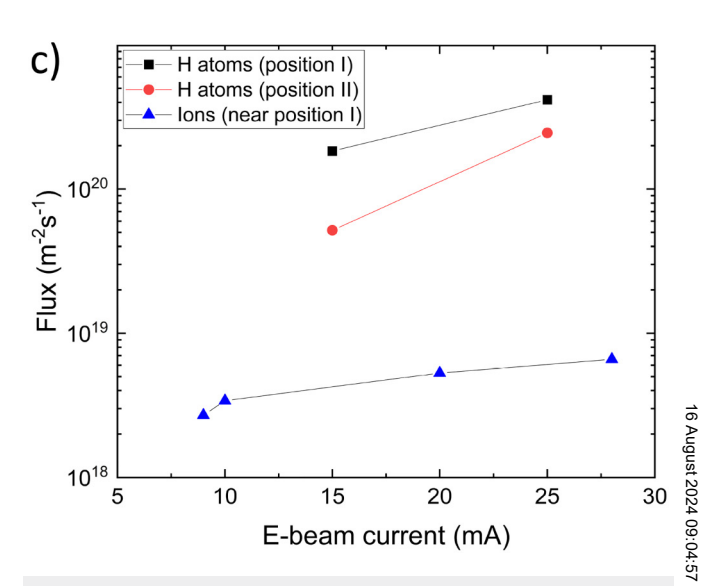


FIG. 4. Photographs of the HFS inside the EBR setup near the 10 mm orifice for two orientations: 1 (a) and 2 (b) obtained by rotating the sensor by 180°. The location of the electron beam is indicated in (b). Recombining H fluxes were measured at the two positions marked with red letters as I and II. (c) Atomic hydrogen fluxes (square and circle symbols) and ion fluxes (triangle symbols) measured for the e-beam generated plasma in 10 Pa of H₂ gas using a 1000 eV beam at various e-beam currents.

done for two orientations of the sensor [see Figs. 4(a) and 4(b)]. Subsequently, atomic hydrogen fluxes were calculated using signals from HFS₁ and HFS₂ recorded at the same position indicated as "I" (closer to the orifice) or "II" (further from the orifice), thus from two separate measurements. The highest recombining radical flux of 4×10^{20} m⁻² s⁻¹ was measured at position I, using an electron beam with 1000 eV electron energy and 25 mA beam current interacting with H₂ gas at 10 Pa. A lower radical flux was measured at a reduced electron current of 15 mA, as shown in Fig. 4(c) (black symbols for position I). Measured H fluxes at position II [further away from the orifice than I, red symbols in Fig. 4(c)] were lower compared to position I. We attribute that to a decreasing electron current density in the divergent beam and scattering of electrons in the H₂ gas. Figure 4(c) also shows ion fluxes measured for the

TABLE I. Overview of the key properties of different types of hydrogen plasma inside an EUV lithography machine equipped with a 250 W LPP source, near the reticle minienvironment (RME) location (from Ref. 2) and off-line setups at TNO.

Plasma type (location/setup name)	H ₂ pressure (Pa)	EUV power (W)	Max ion flux (m ⁻² s ⁻¹)	Peak ion energy (eV)	H (radical) flux (m ⁻² s ⁻¹)	Radical-to-ion ratio	Source frequency (Hz)	Pulse duration (s)
EUV-generated (RME) ²	5	50	~10 ¹⁷	<10	~10 ¹⁹	~100	50 000	<10 ⁻⁸
EUV-generated (EBL2, TNO) ⁵	5-40	4.2	8×10^{17} (at 20 Pa)	1-8	$< 7 \times 10^{18a}$ (at 20 Pa)	<10	1000-3000	<10 ⁻⁸
ECR (SoX, TNO)	5-10	_	2×10^{19}	5-10	7×10^{20a}	35	CW	CW
E-beam generated (EBR, TNO)	1–10	_	6×10^{18} (CW mode)	2–10	1×10^{21a} (CW mode)	167	1-100 000	$4 \times 10^{-8} - 1$

^aPlease note that the total H radical flux was calculated from recombining H fluxes measured with the HFS and using the γ_{Pt} = 0.3.

e-beam-generated plasma in 10 Pa of H2 gas, using 1000 eV electron energy and varying electron beam current. In these measurements, the RFEA was mounted close to position I. It can be seen that the flux of recombining hydrogen is nearly two orders of magnitude higher than the hydrogen ion flux.

C. Comparison to other experimental setups

Table I summarizes plasma properties in an EUV lithography machine near the so-called reticle mini-environment for a 250 W LPP source (from Ref. 2) and for three plasma setups at TNO. The EBL2 facility at TNO uses a LDP source to generate high intensity EUV pulses, which ionize hydrogen gas in the exposure chamber. The EUV-generated plasma in EBL2 shows similar peak ion energies as the scanner plasma and allows for accelerated lifetime testing due to its high peak intensity and high ion flux. The EBL2 facility is available for external customers to conduct experiments on plasma/EUV-material interactions under nearly realistic scanner conditions. Nevertheless, this setup might not be ideal for some feasibility studies and exploratory tests due to its complexity and

For such purposes, typically non-EUV plasma setups are used, which are more straightforward to implement and more costefficient. For example, ECR plasma sources might be considered for material lifetime testing due to high ion fluxes and ion peak energies below 10 eV. Drawbacks of such setups are a lack of EUV photons, a low radical-to-ion ratio and the presence of the source head in the exposure chamber, which can result in significant Si contamination when not properly shielded. Moreover, the CW mode of operation of the Aurawave ECR source, used in TNO setups, results in a continuous plasma, which lacks the temporal behavior of the pulsed-EUV-generated plasma.

As shown in the previous sections, the e-beam generated plasma at the EBR setup shares many similarities with the pulsed-EUV-plasma inside EUV lithography machines in terms of ion and radical fluxes, peak ion energy, and radical-to-ion ratio. Moreover, the used e-gun can be operated both in CW and pulsed mode with tunable pulse duration and frequency. In this way, dynamic properties of the EUV-generated plasma can be mimicked.

The lack of EUV photons at the EBR setup is an obvious drawback, but in the past, research has shown that electron beams can be used to mimic EUV photons in processes like carbon growth or oxidation of Ru coatings. 13,14 Currently, we are investigating whether electron beams can mimic properties of EUV photons for different EUV-induced processes, also for materials other than Ru coatings.

IV. SUMMARY

In this paper, we presented a novel experimental setup at $\frac{1}{2}$ TNO, which uses a high-pressure, high-current electron beam gun to produce low-temperature hydrogen plasma by means of \(\frac{1}{2} \) electron-impact ionization. An e-beam with 1000 eV electron 8 energy and 25 mA beam current was used to generate an ion flux 5 of $\phi_{\rm ion} = 6 \times 10^{18} \ {\rm m}^{-2} \ {\rm s}^{-1}$ with a peak ion energy of 2 eV and a maximum recombining radical flux of $\phi_{{\rm rec},H} = 4 \times 10^{20} \ {\rm m}^{-2} \ {\rm s}^{-1}$. We showed that this e-beam generated plasma resembles the EUV-generated plasma in several key properties, e.g., the ion flux, radical flux, peak ion energy and radical-to-ion ratio. Additionally, the possibility of producing a pulsed plasma with a variable pulse duration (400 ns-1 s) and repetition rate (1-100 000 Hz) allows to reproduce the temporal behavior of the EUV-generated plasma. The generation of pulsed plasmas is a unique feature of the EBR setup that distinguishes it from other non-EUV test setups and due to multiple similarities with the scanner plasma, the setup is suitable for testing materials and EUV components prior to their use inside lithographic machines. Therefore, we consider the EBR setup as a complementary machine to the existing EUV setups (like EBL2) for lifetime testing of optics and materials.

ACKNOWLEDGMENTS

We would like to thank Jurjen Emmelkamp, Norbert Koster and Martayasa Putra for their contributions in designing the EBR setup. This work was supported by the ECSEL Joint Undertaking (JU) under Grant Agreement No. 875999. The JU receives support from the European Union's Horizon 2020 Research and Innovation Program and Netherlands, Belgium, Germany, France, Austria, Hungary, United Kingdom, Romania, and Israel.



AUTHOR DECLARATIONS

Conflict of Interest

The authors have no conflicts to disclose.

Author Contributions

A. S. Stodolna: Conceptualization (equal); Data curation (supporting); Formal analysis (supporting); Investigation (lead); Supervision (equal); Writing – original draft (lead). T. W. Mechielsen: Conceptualization (equal); Data curation (lead); Formal analysis (equal); Investigation (supporting); Writing – review & editing (equal). P. van der Walle: Conceptualization (equal); Data curation (supporting); Investigation (supporting); Supervision (equal); Writing – review & editing (equal). C. Meekes: Data curation (supporting); Formal analysis (equal); Investigation (equal); Writing – review & editing (equal). H. Lensen: Conceptualization (supporting); Project administration (lead); Writing – review & editing (equal).

DATA AVAILABILITY

The data that support the findings of this study are available from the corresponding author upon reasonable request.

REFERENCES

- ¹C. Luo, C. Xu, L. Lv, H. Li, X. Huang, and W. Liu, RSC Adv. 10, 8385 (2020).
 ²M. van de Kerkhof, A. Yakunin, D. Astakhov, M. van Kampen, R. van der
- M. van de Kerkhof, A. Yakunin, D. Astaknov, M. van Kampen, R. van der Horst, and V. Banine, J. Micro-Nanolith. MEMS MOEMS 20, 033801 (2021).

 30. V. Braginsky et al., J. Appl. Phys. 111, 093304 (2012).
- ⁴J. van Veldhoven, C. C. Wu, A. J. Storm, M. van Putten, J. R. Meijlink, and A. G. Ushakov, J. Vac. Sci. Technol. B 41, 012603 (2023).
- ⁵S. G. Walton, C. Muratore, D. Leonhardt, R. F. Fernsler, D. D. Blackwell, and R. A. Meger, Surf. Coat. Technol. 186, 40 (2004).
- ⁶D. Leonhardt, C. Muratore, S. G. Walton, D. D. Blackwell, R. F. Fernsler, and R. A. Meger, Surf. Coat. Technol. 177–178, 682 (2004).

- ⁷M. Ryoji, T. Hara, K. Ohnishi, M. Hamagaki, Y. Dake, and M. Tohkai, Jpn. J. Appl. Phys. 31, 4357 (1992).
- ⁸C. Muratore, S. G. Walton, D. Leonhardt, R. F. Fernsler, D. D. Blackwell, and R. A. Meger, J. Vac. Sci. Technol. A 22, 1530 (2004).
- ⁹E. M. Oks, A. V. Tyunkov, Y. G. Yushkov, and D. B. Zolotukhin, Surf. Coat. Technol. 325, 1 (2017).
- 10 E. H. Lock, D. Y. Petrovykh, P. Mack, T. Carney, R. G. White, and S. G. Walton, Langmuir 26, 8857 (2010).
- ¹¹S. G. Walton, S. C. Hernández, D. R. Boris, T. B. Petrova, and G. M. Petrov, J. Phys. D: Appl. Phys. **50**, 354001 (2017).
- ¹²C. Muratore, S. G. Walton, D. Leonhardt, and R. F. Fernsler, J. Vac. Sci. Technol. A 24, 25 (2006).
- ¹³N. Koster, B. Mertens, R. Jansen, A. van de Runstraat, F. Stietz, and M. Wedowski, Microelectron. Eng. 61, 65 (2002).
- ¹⁴M. E. Malinowski, C. A. Steinhaus, D. E. Meeker, W. M. Clift, L. E. Klebanoff, and S. Bajt, Proc. SPIE 5037, 429 (2003).
- 15 J. van Veldhoven, A. S. Stodólna, A. Storm, J. van den Brind, N. Geerits, and J. Vlaar, IEEE Trans. Plasma Sci. 49, 3132 (2021).
- ¹⁶J. Stortelder, R. Ebeling, C. Rijnsent, M. van Putten, V. de Rooij-Lohmann, and M. Smit, Proc. SPIE 11854, 1185414 (2021).
- 17J. A. Herron, S. Tonelli, and M. Mavrikakis, Surf. Sci. 614, 64 (2013).
- 18S. G. Walton, D. R. Boris, S. C. Hernández, E. H. Lock, T. B. Petrova, and G. M. Petrov, ECS J. Solid State Sci. Technol. 4, N5033 (2015).
- ¹⁹Y. K. Kim and M. E. Rudd, Phys. Rev. A **50**, 3954 (1994).
- ²⁰J. S. Yoon, M. Y. Song, J. M. Han, S. H. Hwang, W. S. Chang, and B. Lee, J. Phys. Chem. Ref. Data 37, 913 (2008).
- ²¹T. H. M. van de Ven, P. Reefman, C. A. de Meijere, R. M. van der Horst, M. van Kampen, V. Y. Banine, and J. Beckers, J. Appl. Phys. 123, 063301 (2018).
- ²²J. F. M. Velthuis, A. Storm, M. van Kampen, R. van der Horst, and H. B. Profijt, J. Vac. Sci. Technol. A 37, 061302 (2019).
- 23 B. J. Wood and H. Wise, J. Chem. Phys. 29, 1416 (1958).
- 24 V. Cremers, R. L. Puurunen, and J. Dendooven, Appl. Phys. Rev. 6, 021302 (2019).
- ²⁵A. D. Tserepi and T. A. Miller, J. Appl. Phys. 75, 7231 (1994).
- ²⁶M. Mozetič, M. Drobnič, and A. Zalar, Appl. Surf. Sci. 144, 399 (1999).
- ²⁷G. Cartry, X. Duten, and A. Rousseau, Plasma Sources Sci. Technol. 15, 479